Laser diagnostics in a diesel engine

E.J. van den Boom, P.B. Monkhouse, C.M.I. Spaanjaars, W.L. Meerts, N.J. Dam, J.J. ter Meulen

Dept. of Applied Physics, Univ. of Nijmegen, The Netherlands

ABSTRACT

Results of laser diagnostics inside a 6-cylinder heavy-duty diesel truck engine are presented. Optical access is obtained by quartz windows mounted in the cylinder head and in the piston. The engine is running on commercial diesel fuel, causing strong attenuation of the UV laser radiation. The sprays are visualized by laser induced fluorescence (LIF) from polycyclic aromatic hydrocarbons present in the diesel fuel. The measurements were focused on the formation of nitric oxide that could be detected by LIF as a function of the crank angle. The fluorescence signals were processed in order to obtain relative NO density curves during the combustion process. Evidence was obtained for the formation of NO between rather than within the spray flames.

Keywords: diesel engine, laser diagnostics, NO formation, diesel spray, LIF

1. INTRODUCTION

Diesel engines arguably power the majority of road transportation vehicles. The prognosis for their future use is that these engines will remain to be used for a long time in the heavy-duty transport business, because they are powerful engines that are the only serious alternative for heavy-duty work. As such, their impact both on economy and on the environment can hardly be underestimated. In many countries, legislation seeks to strike a balance between the demands for increased capacity and for reducing adverse effects on the environment. The various constituents present in the exhaust gases contribute to the waste of our natural surroundings. To this end, emission regulations are imposed that, more or less in pace with expected technological advances, become more stringent every few years. Up to the present, engine manufacturers can meet these ever more stringent legislative requirements. Reduction of the polluting exhaust gases can be performed after the gases have left the engine, so-called catalyst after-treatment in the exhaust pipe and/or by adapting the engine and the operating conditions in such a way that less harmful constituents will be emitted. The lack of detailed, fundamental knowledge about the diesel combustion process itself becomes ever more evident. Of course, this scantiness of basic knowledge is for a large part due to the extreme complexity of (multi-component) diesel fuel combustion, which typically takes place under conditions hardly amenable to experimental analysis.

Nevertheless, several research groups are involved in studying details of combustion in diesel engines, most often using laser-based techniques in order to minimize perturbations of the process (see e.g. ref. 1 - 7). Compression-ignition engines running under realistic conditions (standard diesel fuel, minimized modification of the combustion chamber) provide very adverse measurement conditions. As a result, most work reported to date concerns diesel engines running on substitute fuel[1] and/or oxygen-enriched intake air[2-4]. Regular diesel fuel and ambient intake air were used in the work of Stoffels *et al.*[5,6], but the engine concerned was considerably modified and not very representative for modern diesel engines. The recent work of Dec and coworkers has led to conceptual views of diesel combustion that partly challenge the "established" views[7,8].

The objective of the present work is to study the nitric oxide formation at specific locations within the combustion chamber of a regular, heavy-duty diesel truck engine under operating conditions as realistic as possible. The engine will be described in some detail, after which spray studies by both natural emission measurements and LIF of polycyclic aromatic hydrocarbons (PAH) present in the diesel fuel will be presented. The paper will be focused on the nitric oxide LIF measurements, which have been performed as a function of engine load and crank angle. Quantification of the results is a main subject of the discussion.

2. EXPERIMENTAL

2.1. Engine

The research engine is a six-cylinder 11.6 liter heavy-duty 4-stroke diesel engine produced by DAF Trucks (Eindhoven, the Netherlands). One of the cylinders has been modified for the experiments as shown in Fig. 1. This cylinder has been elongated by 40 cm, to provide access to the head. The latter corresponds to the DAF XF 95 series, a 4-valve head with central 6- or 8-hole injector and symmetrical configuration. One outlet valve has been removed, and in this position either a pressure transducer (AVL QHC32) or a quartz observation window (referred to as 'top window') can be mounted. Three other rectangular (47.5×22.5 mm^2) quartz windows are mounted in the sides of the cylinder head, providing optical access to the uppermost part of the combustion chamber at all times during a stroke.

The piston in the measurement cylinder consists of an elongation bolted onto the original piston. The elongation can be capped either by an original mexican-hat type crown of aluminum alloy, or by a flat-bowl crown with a quartz bottom part. The latter provides full optical access to the central 74 mm of the combustion chamber (bore 130 mm). Light emitted through the piston window can be observed through slots in the side of the piston elongation and in the side of the cylinder wall via a 45° mirror that can be shifted into the engine during operation. In order to reduce soot formation the elongated piston runs without lubrication. Intake air temperature and boost pressure as well as cooling water temperature are all continuously controlled and electronically adjustable. Break load is provided by a water-cooled dynameter.

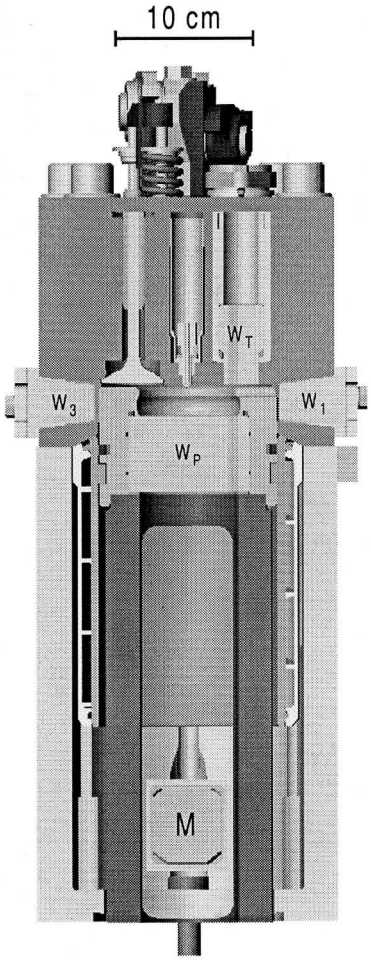

Fig.1: Schematic drawing of the optically accessible cylinder of the DAF diesel truck engine (cross section of the measurement cylinder). $W_{1,3}$: side windows (W_2 not visible); W_T: top window; W_P: piston window; M: mirror under 45° that can be shifted into the elongation during operation of the engine.

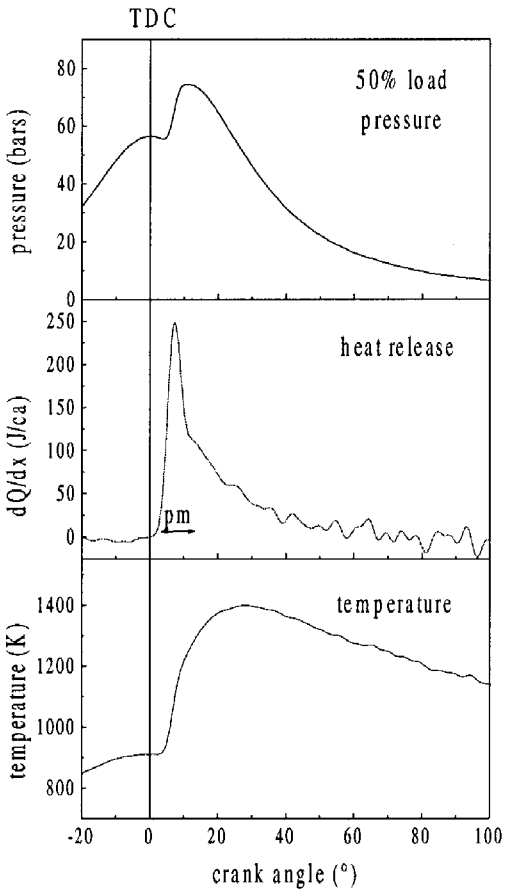

Fig. 2. In-cylinder pressure (upper panel), heat release rate (in Joule per degree crank angle; middle panel) and mean gas temperature (for 313 K inlet air temperature; lower panel) for the measurement cylinder of the engine running at 50% load. The premixed burn phase (pm) is indicated in the heat release panel.

All experiments are performed with the engine running on commercial low-sulfur "City diesel" fuel, obtained from a local retailer. (The same fuel is used for the public transportation buses in Nijmegen.) Dehumidified ambient air is used as intake air. The engine runs in skip-fired mode (typically 1:20 to 1:40) in order to avoid excessive heating of the (non-lubricated) measurement cylinder.

Steady-state conditions are simulated by preheating the combustion chamber by the cooling water. Fuel injection starts at 3° bTDC and the combustion starts at about 1° to 5° aTDC, depending on the load. The compression ratio varies between $\varepsilon = 15.5$ (aluminum crown) and $\varepsilon = 15$ (quartz-bottom crown); in the unmodified engine $\varepsilon = 16$. The pressure, temperature and heat release curves for the 50% load case are given in Fig.2. Note that the relatively late start of injection results, at this load, in a small ignition delay (about 4.5°). The heat release is dominated by the premixed burn, with only a small contribution from the diffusion flame.

2.2. Optical

Laser induced fluorescence of NO is induced in the A $\leftrightarrow$ X band, using 226 nm radiation for excitation (A(v'=0) $\leftarrow$ X(v"=0)) and several higher wavelength bands (A(v'=0) $\rightarrow$ X(v"=1-3)) for detection. Laser radiation is derived from a Nd:YAG-pumped pulsed dye laser (Continuum PowerLite 9010 @ 355 nm; Λ Physik ScanMate 3 @ Coumarin 47 or Coumarin 2). Scattered light is detected through an imaging monochromator (ARC SpectraPro 300i) by an intensified CCD camera (Princeton Instruments, ICCD 576G/RB-E; 16 bits)), a combination which essentially constitutes an optical multichannel analyzer.

Additional suppression of elastically scattered radiation, so-called Mie signal, was, when necessary, achieved by including a normal incidence high reflector coated for 226 nm or a UG5 filter in the detection beam path. The mirror that can be shifted into the cylinder (M in figure 7.2.1.1 is a high reflector for the 225-260 nm wavelength range (Laser Optik, Garching, D). The use of a spectrograph rather than transmission filters is advantageous for several reasons. The wavelength selectivity of a spectrograph is superior to that of filters, and can be adjusted by choosing different gratings. Also, spectroscopic interference by other combustion products is monitored automatically, and can be avoided with certainty during the whole measurement.

The various optical access ports of the engine allow for a flexible configuration of the excitation and detection optics, and several different schemes have been used to obtain the results presented below. Illumination is effected either through the side window W_1 (closest to the top window) or through the piston window. Fluorescence is detected through the piston window, the top window or the side window W_2.

For transmission measurements the laser beam entered the engine through side window W_1 and the transmitted radiation was detected by a CCD camera behind W_3. The total transmission therefore includes absorption by the windows. Visual inspection showed the side and top windows to remain clear even after prolonged operation of the engine. Only the piston window was slowly covered by a thin gray layer, starting at the edges where the sprays hit the combustion bowl. In the course of an engine run this gray deposit slowly grows inwards, but it has been verified that fluorescence signal levels from various locations within the combustion chamber remain steady over hundreds of work cycles (engine firing 1:40). Since the attenuation of laser radiation and induced fluorescence within the combustion chamber is expected to be a main concern in LIF experiments, transmission measurements have been performed at several engine loads. Representative curves for the relative transmission of 226 nm radiation through half the combustion chamber for 50% and 90% load are shown in Fig. 3. Relative transmission is defined here as the ratio of measured transmission through the firing engine versus that of the motored engine, so that window absorption is accounted for. The figure shows a strong decline of the transmission as soon as fuel injection starts (note the logarithmic ordinate), which recovers much later in the stroke. The fuel injection rate at 90% load is larger than that at 50% load, which probably explains the deeper transmission minimum in the former case. Later in the stroke, however, the combustion chamber becomes more transparent in the 90% load case, possibly due to the higher temperatures maintained for a longer time, that can be expected to result in more complete soot burn-out. The large impact that (commercial) diesel fuel injection has on the transmission of 226 nm radiation poses a violent contrast to the negligible effect that low-sooting diesel fuel is reported to have.

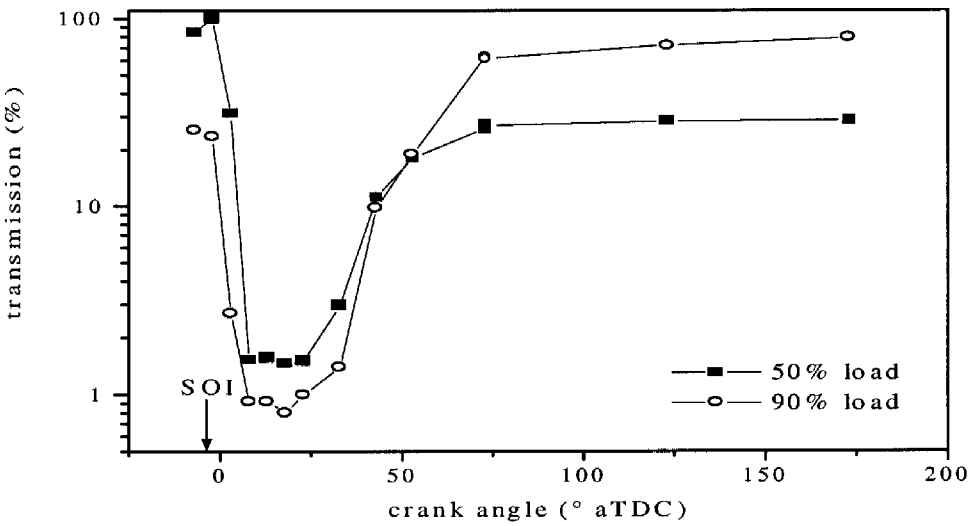

Fig. 3. Relative transmission of 226 nm radiation through the first half part of the firing engine (relative to that of the motored engine) for two different loads calculated from transmission measurements performed through the entire combustion chamber through the side windows under the assumption that the combustion is symmetrically distributed relative to the injector position. Start of injection (SOI) is indicated. An 8-hole injector is used.

3. RESULTS

3.1. Spray visualization

The LIF technique can be applied to excite the PAH molecules present in the diesel fuel to visualize the exact start and end of the diesel injection. In addition, the position where the combustion starts can be compared to the position of the diesel sprays. A 90 mJ/pulse laser beam at 355 nm has been used to excite 3 and 4 ring PAH molecules in the diesel fuel. The laser beam enters the combustion chamber through the piston window via the aluminum coated mirror placed underneath it (see Fig. 4). The piston window was illuminated as homogeneously as possible. The natural flame emission and the LIF originating from the PAH molecules are detected through the piston window via the same mirror, using two ICCD cameras with different spectral filters in front of them. The light is distributed over the two cameras by using a quartz plate as beam splitter. The light traversing this plate towards the ICCD camera detecting the LIF signal, is passing a filter combination effectively transmitting a wavelength band between 400 and 520 nm. The light reflected by the quartz plate is filtered by a long wavelength pass filter, blocking light below 435 nm, and is detected by the ICCD camera used for the imaging of the natural flame emission.

The images resulting from the LIF and natural flame emission have been recorded almost simultaneously (natural flame emission images are recorded 125 ns after the LIF images) for various crank angles. In Fig. 5 images measured at 4° aTDC are shown for 75% engine load. In the middle of the LIF image a star-like structure is visible. This structure is present from 2° bTDC till 16° aTDC and is caused by PAH molecules in the diesel fuel sprayed into eight directions. The eight clouds in the right hand image show up at angles larger than 1° aTDC and are due to the natural flame emission of the combustion. Both LIF and natural flame emission are visible in the left image of Fig. 5, because the natural flame emission of the diesel combustion cannot be suppressed completely in the LIF measurements. From these measurements it was concluded that combustion starts

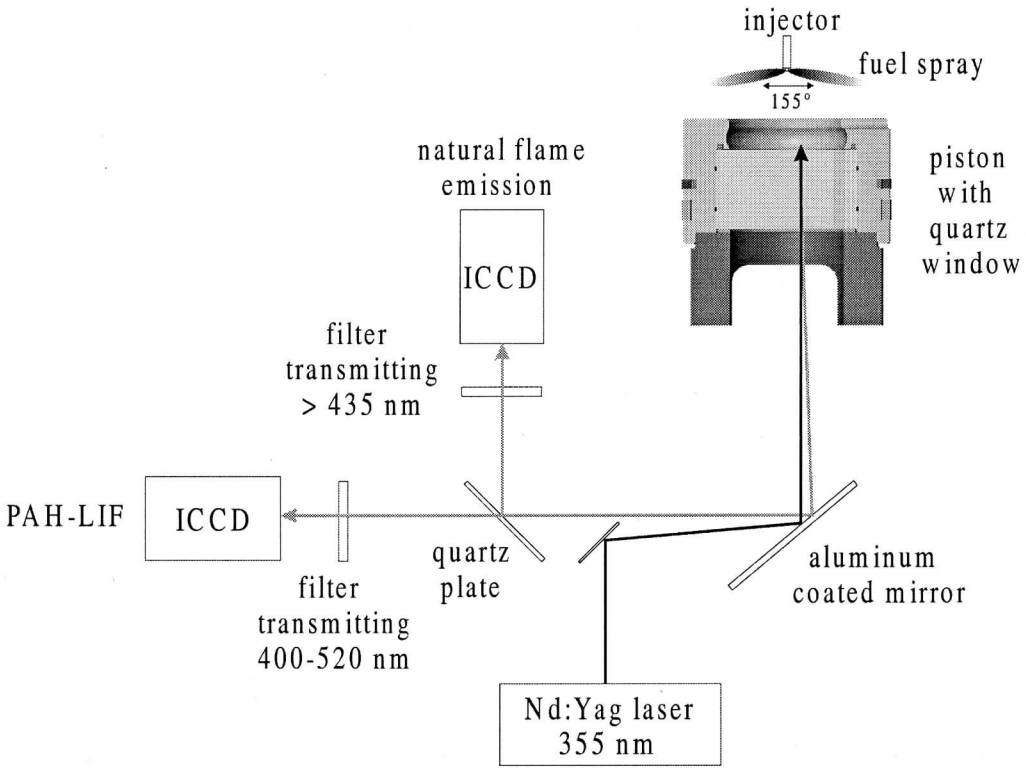

Fig. 4. Experimental setup for PAH-LIF and natural emission measurements. The diesel is sprayed into the combustion chamber under an angle of 155° between opposite sprays.

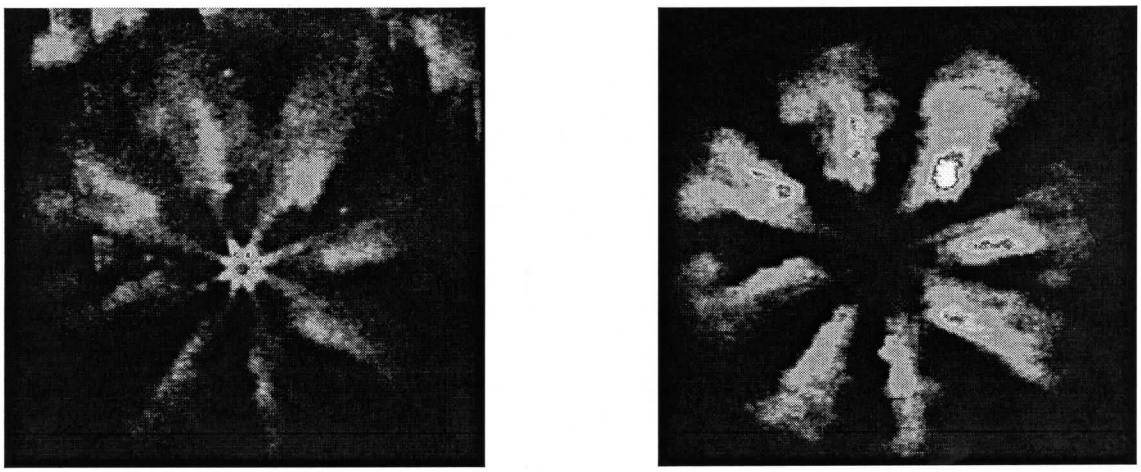

Fig. 5. LIF originating from PAH molecules in the diesel fuel (left hand side) and natural flame emission (right hand side) measured simultaneously at 4° aTDC and at 75% engine load.

at about 1° aTDC. At higher engine load the combustion starts earlier. At 10%, 50% and 75% engine load combustion starts at 5°, 4° and 1° aTDC respectively. From measurements not depicted one can derive that combustion also ends later for higher loads. The length of the area from which the LIF signal is observed is only 18 mm. A close inspection reveals that the decrease of the fluorescence intensity with the radial distance r from the injector is faster than the expected decay with r^{-1}. This is probably caused by the evaporation of the PAH molecules from the liquid part of the spray.

From Fig. 5 it can be seen that the combustion does not start in the direction of the diesel spray, but off-axis. It turns out that the combustion starts at one side of the diesel spray, as a consequence of the swirl, i.e. the air flow in the combustion chamber in the tangential direction, which is in clockwise direction in the image.

3.2. NO LIF measurements

3.2.1. NO excitation through the side window

NO fluorescence measurements have mostly been performed at the 226.037 nm excitation (Q_1 + $P_{21}(14)$ and Q_2 + $R_{12}(21)$), initially with the 2 mJ/pulse laser beam entering the combustion chamber through the side window W_1 and fluorescence detection through the top window. In these measurements the standard aluminum piston crown was used. This configuration has the advantage of a small path length of both laser beam and fluorescence inside the combustion chamber, but has the disadvantage that the top window offers only a limited view of the combustion bowl. In this setup NO is observed from 30° aTDC onwards. From 58° aTDC onwards more NO seems to be present in the combustion bowl than in the squish region. The reason that no NO fluorescence is detected at crank angles smaller than 30° aTDC is that the laser beam hardly enters the field of view, because of the low transmission through the combustion chamber for crank angles between TDC and 30° aTDC.

Figure 6 presents raw NO fluorescence data (curve □) as a function of crank angle. The data correspond to averages over five successive engine cycles integrated over the field of view of the top window. Single shot data scatter around the average by about 10-50%. Fluorescence could be observed (in the averages) from 30° aTDC onwards. In order to transform the raw

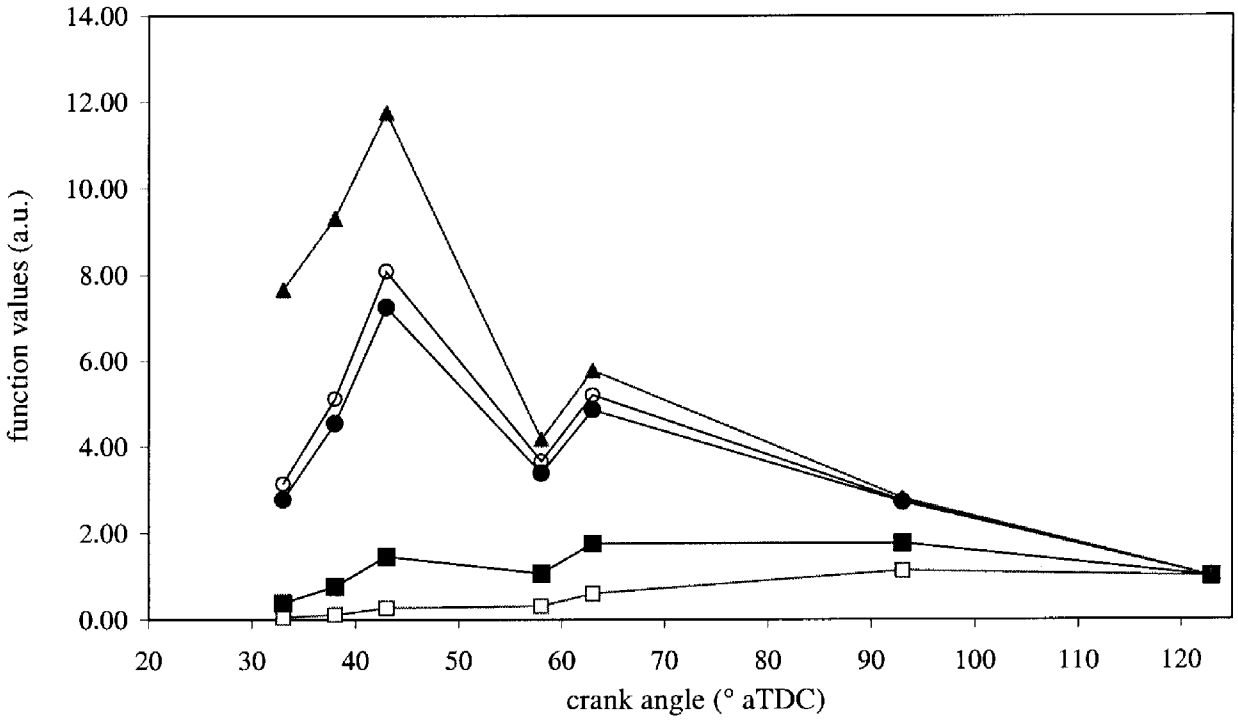

Fig. 6. NO fluorescence intensities as a function of crank angle (curve □) measured at 50% engine load using a 6-hole injector and the corresponding NO densities (curve ▲). The other curves correspond to various stages of the correction procedure that transforms the fluorescence signal into density (see text). The raw signal (□) is successively corrected for quenching (■) plus excitation efficiency (●) plus Boltzmann fraction (O) plus finally attenuation (▲). The signal-to-noise ratio in the raw data varies from about S/N=2 at 33° aTDC to 40 at 123° aTDC.

fluorescence data into NO densities, they must be processed for the effects of *i*) collisional fluorescence quenching (incl. Electronic Energy Transfer (EET)), *ii*) the absorption line width, *iii*) the varying thermal population of the probed energy level (Boltzmann fraction) and *iv*) the in-cylinder attenuation. The successive effects of these corrections are included in Fig. 6.

Contrary to previous work of our group[5,6], in which a 193 nm excimer laser was used to excite the D(v'=0) ← X(v''=1) band, the correction for the Boltzmann fraction is now of minor importance (compare curves ● and O). Another difference with the 193 nm excitation scheme lies in the collisional quenching correction. Quenching of the NO $D^2\Sigma^+$-state is expected to be dominated by N_2 collision-induced EET to the A-state[9]. Quenching of the (lowest electronically excited) $A^2\Sigma^+$-state, on the other hand, is hardly affected by collisions with N_2, but depends on collision partners like O_2, CO_2, H_2O and hydrocarbons[10-12]. With the known quenching cross sections and estimated concentrations of the major chemical species in the combustion chamber, quenching rates Q have been calculated. Temperature and pressure dependencies were found to be well described by the relationship $Q \propto P \cdot T^{-1/2}$, with P the total pressure. This relation has subsequently been used in correcting the fluorescence data. As expected, Fig. 6 shows the quenching correction to be substantial (compare curves □ and ■), especially at lower crank angles. Another important factor is to be found in the varying excitation efficiency (compare curves ■ and ●), which is mainly due to the absorption line width. Both the laser and the absorption line profiles are here assumed gaussian, with widths (FWHM) of $\Delta_L = 0.15$ cm^{-1} and $\Delta_{abs} = 0.58.P.(295/T)^{0.75}$ cm^{-1} (total pressure P in bars, T in K)[14,15], respectively. Because of the small path length that the light has to cover in the setup used, the attenuation correction (using the 226 nm transmission data of Fig. 2 for the 247 nm fluorescence as well) is seen to have only a relatively small effect (compare curves O and ▲). The net effect of all processing factors is a change of the roughly monotonically rising raw data curve (□) into a NO density curve (▲) that shows a maximum for small crank angles (close to the detection limit, in fact). Concerning the decline of the density curve

towards larger crank angles, it should be noted that the trivial effect of the expanding in-cylinder volume has not been incorporated in Fig. 6 (which displays density rather than amount).

A series of NO density curves obtained for different engine runs on different days is presented in Fig. 7. In all cases the excitation laser beam entered the engine through the side window W_1 (but in various lateral positions) and the fluorescence was detected either through the top window (▲-curve; from Fig. 6) or through the side window W_2 (other curves); the attenuation correction was modified accordingly. Most data points correspond to averages over several engine cycles (the number n is indicated in the figure). Excitation on the $Q_2 + Q_{12}(14)$ at 226.373 nm [16] was used for one of the curves (O); for the others the scheme mentioned above was used. The single shot data (□) showed NO fluorescence only from 40° aTDC onwards. At 123° aTDC the NO density is assumed to be equal for all the curves using the same injector, because at this crank angle the combustion gas is assumed to be fully mixed to such an extent that the measured NO density should probably not differ anymore for different geometries of excitation and detection. The NO density curves corresponding to the measurements performed with the 8-hole injector correspond with each other rather well in shape and in absolute values, as do the curves for the 6-hole injector within the scatter of the single shot data. The measurements using the different injectors cannot be compared with each other, because the NO production might be different for the two different operating conditions.

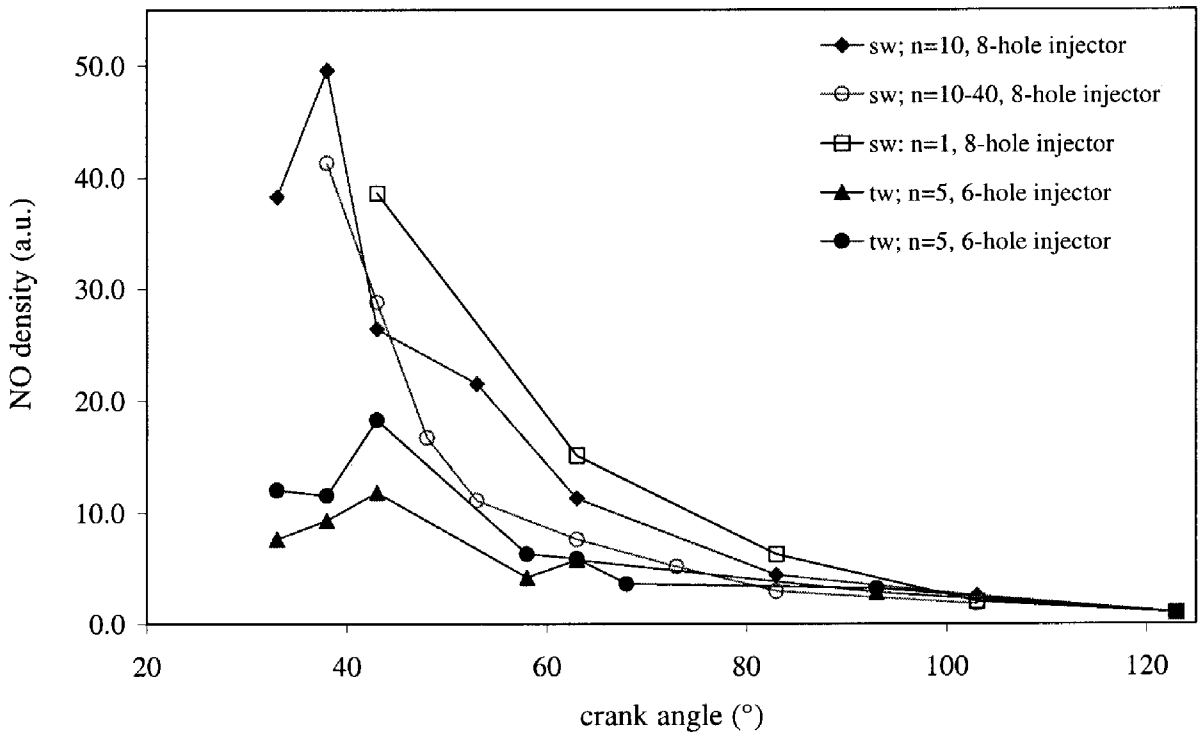

Fig. 7. Several NO density curves obtained during different engine runs and several optical configurations (see text). sw = side window detection; tw = top window detection; n = number of engine cycles over which is averaged. All curves are determined at 50% engine load. All curves are rescaled to one at 123° aTDC. In spite of the fact that the curves obtained using the 6-hole injector should not be compared with those obtained using the 8-hole injector, all curves have been normalized to unity at 123° aTDC.

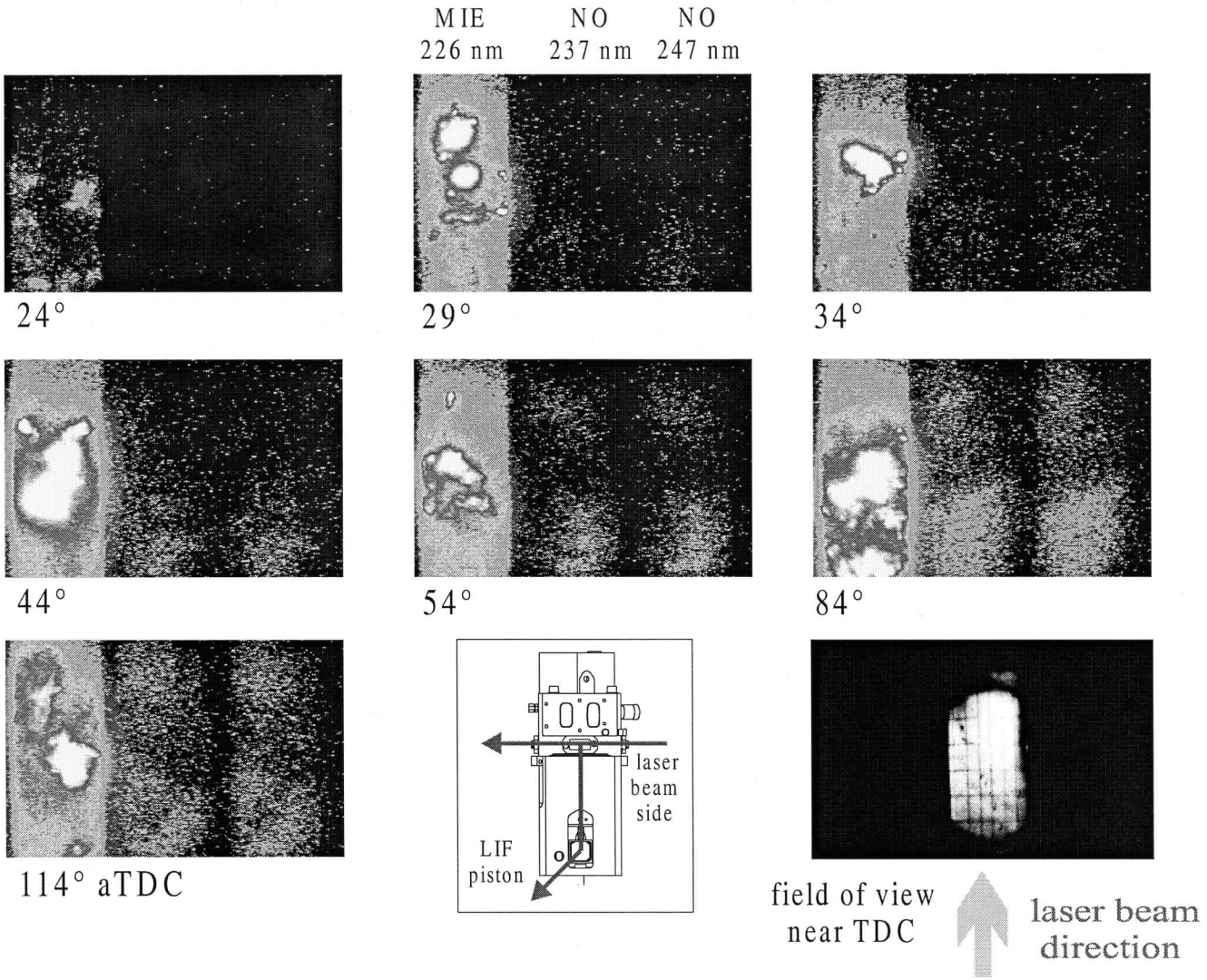

Fig. 8. Mie scattering at 226 nm and NO fluorescence from the A(v'=0) → X(v"=1,2) band at 237 and 247 nm simultaneously measured single shot in the so-called imaging mode as a function of crank angle at 10% engine load using an 8-hole injector. The image in the right bottom corner shows the viewed part of the combustion chamber at the 0^{th} order of the monochromator through the piston window: a piece of paper with lines in a rectangular shape was put upon the piston. The intensities of all images are rescaled on a logaritmic intensity scale to the same maximum value. The white spots in the Mie part of the images are spots with a high scattering intensity and are caused by this rescaling. Signal is present outside the field of view through the piston window positioned at TDC, because of the downwards movement of the piston.

It was observed that more soot is present at the side windows in the combustion chamber where the laser beam enters the combustion chamber using the 6-hole injector. Since transmission data for the engine running with the 6-hole injector could not yet be determined, the raw fluorescence data of the measurements performed with the 6-hole injector have been corrected using the transmission data for the 8-hole injector. This implies that the NO densities for the 6-hole injector, are underestimated. The use of a different injector will probably result in a different course of the combustion process, resulting in different NO densities.

Figure 8 shows simultaneously recorded Mie scattering and NO A(v'=0) $\rightarrow$ X(v"=1,2) fluorescence images measured single shot in the so-called imaging mode as a function of crank angle at 10% engine load. The laser beam traverses the combustion chamber through the side windows and the scattered light is detected through the window in the piston. A 7 mm high slot has been made in the piston wall at the side where the laser beam enters the combustion chamber, so the laser beam can traverse the combustion chamber underneath the injector to prevent scattering signals from the injector. The compression ratio was kept the same. NO is detected from 29° aTDC onwards. The Mie scattering signals in the measured images from Fig. 8 show a very large Mie scattering signal present from 29° aTDC onwards, but almost no signal at 24° aTDC: the laser beam hardly traverses the combustion chamber and no NO can be detected at smaller crank angles.

3.2.2. NO excitation and detection through the piston window

A much more detailed view of the combustion is obtained by looking from below, using the piston with the quartz bottom plate. Figure 9 shows a partial view (of the combustion, recorded through the monochromator (grating in 0^{th} order) at 14° aTDC. The position of the injector is indicated at the right, with the 8 jet axes, four of which give rise to the spray flames visible in Fig. 9. The large white circle in the image indicates the rim of the piston window. If the unfocussed laser beam enters the combustion chamber through the piston window as well, it is possible to probe the combustion chamber contents along a line of sight, typically a cylinder with a diameter corresponding to that of the laser beam (about 3 mm) and a height that, in principle, is limited by the distance z_p from the upper side of the piston window to the cylinder head. In practice, however, the penetration depth is often limited by in-cylinder attenuation. Fluorescence is detected through the monochromator at 259 nm (A(v'=0) $\rightarrow$ X(v"=3)). This configuration has the disadvantage that spatial resolution is lost along the line of sight, but is, for the present purpose, outweighed by the fact that the laser beam enters the observation volume immediately, so that attenuation losses (of both laser beam and fluorescence) are kept to a minimum. Three locations for the probe volume are indicated in Fig. 9; the size of the white disks roughly corresponds to the diameter of the laser beam. Points **a** and **c** lie along one of the spray axes (or, rather, along the plume of visible combustion, which is rotated clockwise by about 10° with respect to the spray direction due to swirl), whereas point **b** is located in between two spray flames.

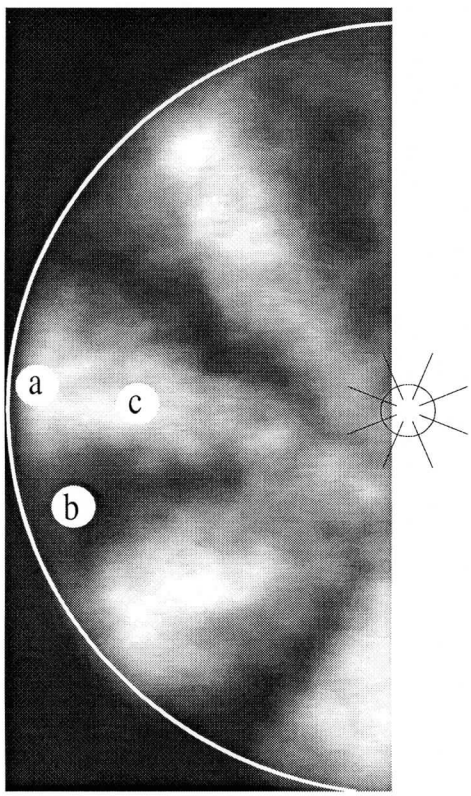

Fig. 9. Location of the sites probed by LIF in the combustion chamber relative to the natural spray flame luminosity (recorded at 14° aTDC). The sites are marked with white circles with a diameter approximately equal to that of the laser beam; the letters are referred to in the text. The flame luminosity is represented in a linear gray scale (white = maximum). At the right the position of the 8-hole injector and the spray directions are indicated.

In this configuration, the earliest unambiguous fluorescence signals from NO could be detected on location **a** (tip of the spray flame) at 14° aTDC, with the engine running at 10% load. Curves for the fluorescence yield (raw data) as a function of crank angle, load and measurement position are given in Fig. 10. Interestingly, the fluorescence yield is lower at 50% load than at 10% load (panel a). Within the spray at 10% load first signs of NO could be detected at 14° aTDC. At 50% load first detectable signals of NO were also observed at 14° aTDC, but only between rather than within the spray flames (panel b). All curves show a steep rise of the fluorescence intensity towards larger crank angles (note the logarithmic ordinate). This rise corresponds well to the rise in transmission shown in Fig. 3, and it therefore seems that, in spite of the favorable optical configuration, the steep rise of the curves in figure 10 is again due to the changing opacity of the combustion chamber contents.

The correction procedure for the laser and fluorescence intensity attenuation is slightly different from the one used for Figs. 6 and 7. This is because an integration along the line of sight must be performed. This could in principle be done along the same lines as discussed above. However, the use of an average absorption coefficient is not a very good approximation for a configuration that probes the early combustion very locally. Indeed, applying the above algorithm to the data of Fig. 10 leads to large scatter in the final data points (data not shown). Therefore, only the raw fluorescence data will be discussed below.

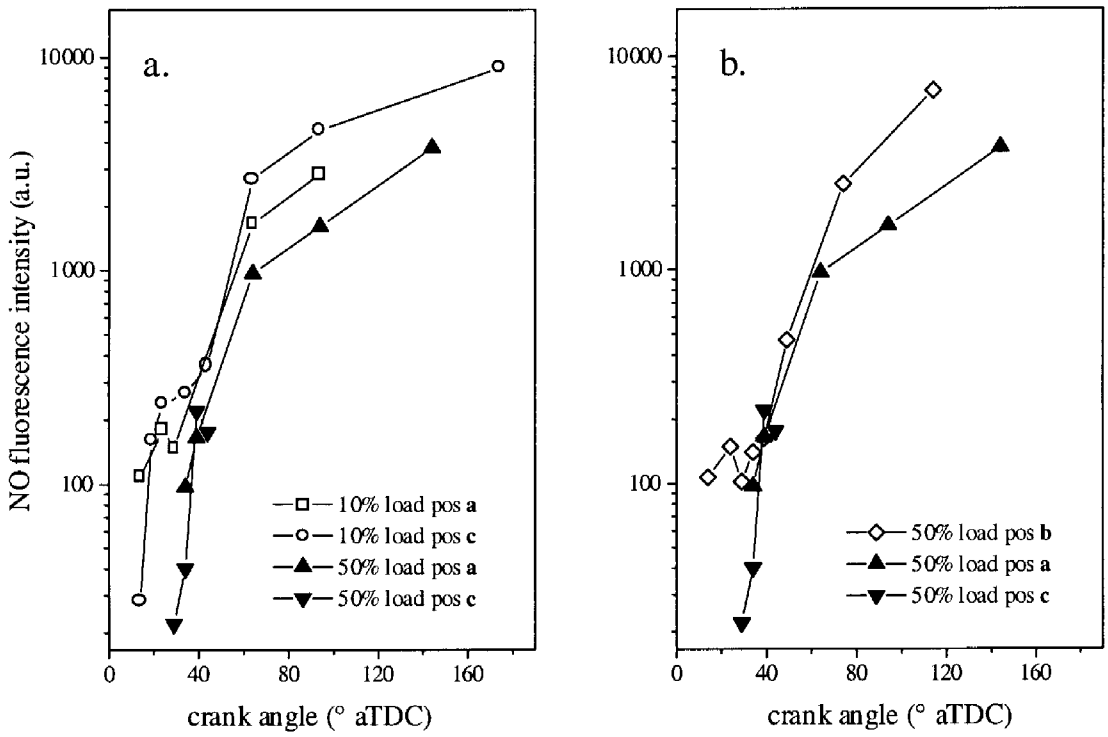

Fig. 10. NO fluorescence yield as function of crank angle, load and probe volume location (see Fig. 9), using illumination and detection both through the piston window. a) Comparison of different loads and probe locations within the spray flames. b) Comparison of probe locations within and between the spray flames. The signal-to-noise ration increases from about 2 (smallest crank angles) to 800 (largest crank angles).

4. DISCUSSION

The results presented above show that laser diagnostics can be applied in a minimally modified combustion chamber of a realistic diesel truck engine (DAF XF 95 series), running on standard commercial diesel fuel. Window fouling did not seriously limit the available measurement time. However, large attenuation was found for the 226 nm radiation early in the combustion stroke, abruptly setting in at start of injection (SOI; Fig. 2). At present it is not clear whether this is due to scattering or absorption. Although we have not run the engine on low-sooting fuel, comparison with literature (notably Ref. 1) suggests that commercial diesel fuel in this respect behaves very differently from low-sooting fuel.

In the spray LIF measurements it was observed that the fluorescing spray has a length of about 18 mm. If this is the liquid spray, before full evaporation, this result is not in disagreement with the result found by Espey *et al.*[17]. He found a penetration depth of the liquid spray of maximally 24 mm, while no droplets were found after 27 mm: all fuel droplets were vaporized. It should be mentioned that Espey *et al.* did not use a real diesel fuel, but a mixture of heptamethylnonane and n-hexadecane. In former measurements Dec and Espey[18] found a penetration depth of the liquid spray of 35 mm, but at lower air temperatures at TDC. This already shows the strong dependence of the liquid spray length on different operating conditions and shows that the result displayed in this chapter are in agreement with measurements performed by other groups. A rough estimation of the liquid spray length of about 25 mm was made by DAF[19]. Several models have been developed to predict the spray structures during injection and/or combustion, for example by Fath *et al.*[20] and Dec[7]. The length of the spray depends on properties as injection pressure, nozzle diameter, cavitation effects at the nozzle, the air temperature, the presence of swirl etc., and cannot be predicted yet as a function of all these different properties. If details about the spray structure and break-up in the DAF engine are desired, additional measurements need to be performed using for example the Mie scattering technique, shadowgraphy or perhaps Schlieren photography. In combination with LIF detection such measurements might reveal much information about the actual spray break-up mechanism. The start of ignition has been seen to occur at the downstream side of the swirl along the spray. The position of the start of combustion relative to the spray axis might be very important for the further development of the combustion process and influence for example the soot and NO_x emissions. Further measurements to study the position of the start of combustion and the subsequent combustion progress through the combustion chamber are needed in combination with NO_x and soot measurements.

NO LIF signals were recorded with several optical configurations. The data processing steps needed to derive density information are in principle well understood, albeit not necessarily straightforward to perform in practice. For fluorescence data obtained relatively late in the combustion stroke ($\Theta \geq 30°$ aTDC) the individual correction steps are illustrated in Fig. 6. The resulting density information was found to reproduce quite well within the experimental accuracy, as illustrated by the data obtained from several engine runs taken weeks apart and different optical configurations (Fig. 7). The curves in Fig. 7 show a NO density that declines with increasing crank angle. Most of the decline can trivially be explained by the increasing combustion chamber volume. However, the curves of Fig. 7 decrease slightly faster, which cannot be caused by a NO conversion into NO_2 [6], since the gas temperature is too high for that process. It might possibly be caused by a mixing of the probed combustion gas with colder gas from other regions near to the side walls of the combustion chamber where probably less NO is formed. In combination with the fluorescence data of Fig. 10, these curves also imply that the NO formation rate possesses a maximum somewhere between 14° aTDC (first signs of NO; Fig. 10) and about 38° aTDC (near the detection limit of the curves in Fig. 6). This maximum therefore occurs after the peak heat release (at 8° aTDC; Fig. 2), at some point during the diffusion burn phase. Although the highest local temperatures will probably be reached during the early spike in the heat release (premixed burn phase), local temperatures in the diffusion flame will still be much higher than the mean gas temperature ($\approx$ 1300 K at 14° aTDC). At this stage, it cannot be decided whether the NO is formed via the thermal (Zeldovich) mechanism or that another (e.g. the Fenimore) mechanism contributes significantly.

An interesting conclusion from the curves in Fig. 10.b is that at 50% load NO is observed earlier between the spray flames (location **b** in Fig. 9) than at the position of the flames (locations **a** and **c**). The difference is at least partly explained by local differences in optical thickness of the cylinder contents this early in the stroke. Between the spray flames the penetration depth of the laser radiation within the combustion chamber is expected to be much larger than at locations where it has to pass through a flame. Qualitative experimental evidence for this is provided by the fact that during measurements at location **b** large back reflections of laser light were often seen, due to scattering of laser radiation on the cylinder head. This hardly ever occurred during measurements at the other two locations. As a result of the larger penetration depth, the probe volume at location **b** is larger than that at positions **a** and **c**. The question remains where the NO between the sprays comes from. It may

of course be formed locally, but it can not be excluded *a priori* that it is formed elsewhere earlier in the combustion and is transported by gas flow to the measurement location. For instance, if it is assumed that NO is formed within the spray flame at position **a** during the peak heat release (at 8° aTDC), where it would probably be invisible for LIF detection due to the limited local penetration depth, gas velocities of about 20 m/sec would be required to transport it to measurement location **b** at 14° aTDC. Although LDA or PIV data on the gas flow velocities in this engine are not available, time-resolved images of the visible combustion (data not shown) do not provide evidence for the occurrence of such flow patterns. However, the luminous soot particles need not be faithful tracers of the gas flow. The swirl number of a XF95 DAF engine is 1.8, measured on a steady state flow test stand without piston[19]. This implies that the gas flow velocity as a result of the swirl will be about 20 m/s at the combustion chamber walls at 65 mm distance from the center of the injector. According to this calculation, a gas flow velocity of about 10 m/s will be present at position **b**. The average piston speed is only about 3 m/sec at these crank angles. If the piston speed, air inlet and compression stroke are included, the gas flow velocity will probably increase, but the value of about 20 m/s will probably not be reached at the positions **a** and **b**. Local formation of NO between the spray flames seems therefore more likely. The oxygen concentration is high, nothing yet being consumed by combustion, and elevated temperatures can be expected because of the vicinity of the flame fronts. Results reported by Dec [Ref. 1, Fig. 4] also provide evidence for early NO formation along the outside of the flame front.

Measurements at earlier injection timing (normal operating conditions for this engine correspond to SOI at 6.2° bTDC) are in progress. Future work will be directed towards improving the detection sensitivity, a more quantitative interpretation of the results and towards correlating local NO densities with those of other combustion products.

ACKNOWLEDGEMENTS

This work is supported by the Dutch Technology Foundation (STW). P.B.M. acknowledges a grant from the EU in the framework of the Marie Curie ptogramme. We gratefully acknowledge DAF Trucks for providing the engine and much advice, as well as Prof. R. Baert (Technical University of Eindhoven), Dr. R. Klein-Douwel (University of Nijmegen), Ir. J. Kruithof (DAF Trucks) and Prof. D. Stapersma (Royal Marine Institute) for enlightening discussions.

REFERENCES

1. J.E. Dec and R.E. Canaan, "PLIF Imaging of NO Formation in a DI Diesel Engine", *SAE paper* no. 980147, 1998
2. H. Nakagawa, H. Endo, Y. Deguchi, M. Noda, H. Oikawa and T. Shimada, "NO Measurements in Diesel Spray Flame Using Laser Induced Fluorescence", *SAE paper* no. 970874, 1997
3. F. Hildenbrand, C. Schulz, V. Sick, G. Josefsson, I. Magnusson and M. Alden, "Laser spectroscopic investigation of flow fields and NO formation in a realistic SI engine", *SAE paper* no. 980148, 1998
4. Th. M. Brugman, G.G.M. Stoffels, N. Dam, W.L. Meerts And J.J. ter Meulen, "Imaging and post-processing of laser-induced fluorescence from NO in a diesel engine", *Appl. Phys. B.* **64**, pp. 717-724, 1997
5. G.G.M. Stoffels, *"Nitric oxide in a diesel engine: laser-based detection and interpretation"*, PhD thesis, University of Nijmegen, 1999
6. G.G.M. Stoffels, E.J. van den Boom, C.M.I. Spaanjaars, N. Dam, W.L. Meerts, J.J. ter Meulen, J.C.L Duff and D.J. Rickeard, "In-cylinder Measurements of NO in a Diesel Engine", *SAE paper* no. 1999-01-1487, 1999
7. J.E. Dec, "A Conceptual Model of DI Diesel Combustion Based on Laser-Sheet Imaging", *SAE paper* no. 970873, 1997
8. P.F. Flynn, P.F. Durrett, G.L. Hunter, A.O. zur Loye, O.C. Akinyemi, J.E. Dec and C.K. Westbrook, *SAE paper* no. 1999-01-0509, 1999
9. H.L.G.J. van den Boom, *"Laser diagnostics in diesel engines"*, PhD thesis, University of Nijmegen, 2000
10. J.W. Thoman Jr, J.A. Gray, J.L. Durant and P.H. Paul, "Collisional electronic quenching of NO $A^2\Sigma^+$ by N_2 from 300 to 4500 K", *J. Chem. Phys.* **97**, pp. 8156-8163, 1992
11. M.C. Drake and J.W. Ratcliffe, "High temperature quenching cross sections for nitric oxide laser-induced fluorescence measurements", *J. Chem. Phys.* **98**, pp. 3850-3865, 1993
12. Y. Haas and G.D. Greenblatt, J. Phys. Chem. **90**, pp. 513-517 (1986)

13. M.R. Furlanetto, J.W. Thomann, Jr., J.A. Gray, P.H. Paul and J.L. Durant, Jr. , J. Chem. Phys. 101, pp. 10452-10457 (1994)
14. A.Y. Chang, M.D. di Rosa and R.K. Hanson, "Temperature dependence of collision broadening and shift in the NO A-X (0,0) band in the presence of argon and nitrogen", *J. Quant. Spectrosc. Radiat. Transf.* **47**, 375, 1992
15. A.O. Vyrodov, J. Heinze and U.E. Meier, "Collision broadening of spectral lines in the A-X (0,0) system of NO by N_2, Ar and heat elevated pressures measured by Laser-Induced Fluorescence", *J. Quant. Spectrosc. Radiat. Transf.* **53**, 277, 1995
16. J. Luque, LIFBASE: database and spectral simulation program (version 1.4), SRI, 1998
17. C. Espey, J.E. Dec, T.A. Litzinger and D. A. Santavicca, " Quantitative 2-D Fuel Vapor Concentration Imaging in a Firing D.I. Diesel Engine Using Planar Laser-Induced Rayleigh Scattering", *SAE paper* no. 940682, 1994
18. J.E. Dec and C. Espey, "Soot and Fuel Distributions in a D.I. Diesel Engine via 2-D Imaging", *SAE paper* no. 922307, 1992
19. T. Straten, (DAF Trucks), personal communication
20 A. Fath, K.-U. M nch and A. Leipertz, *"Spray Break-Up Process of Diesel Fuel Investigated Close to the Nozzle"*, Proceedings of ICLASS-'97, Korea, pp. 513-520, 1997